Studies of Pyrroloquinoline Quinone Species in Solution and in Lanthanide-dependent Methanol Dehydrogenases

Al Danaf, N.; Kretzschmar, J.; Jahn, B.; Singer, H.; Pol, A.; Op Den Camp, H. J. M.; Steudtner, R.; Lamb, D. C.; Drobot, B.; Daumann, L. J.;

Originally published:

June 2022

Physical Chemistry Chemical Physics 24(2022), 15397-15405

DOI: https://doi.org/10.1039/D2CP00311B

Studies of Pyrroloquinoline Quinone Species in Solution and in Lanthanide-dependent Methanol Dehydrogenases

Nader Al Danaf[a,b]†, Jerome Kretzschmar[c]†, Berenice Jahn[a], Helena Singer[a], Arjan Pol[d], Huub J.M. Op den Camp[d], Robin Steudtner[c], Don C. Lamb[a,b], Björn Drobot*[c] and Lena J. Daumann*[a]

[a] Department of Chemistry

Ludwig-Maximilians-University Munich

Butenandtstraße 5 – 13, 81377 München (Germany)

[b] Center for NanoScience

Ludwig-Maximilians-University Munich

Geschwister-Scholl Platz 1, 80539 München (Germany)

[c] Institute of Resource Ecology

Helmholtz-Zentrum Dresden-Rossendorf e.V.

Bautzner Landstraße 400, 01328 Dresden (Germany)

[d] Department of Microbiology

Radboud University

Heyendaalseweg 135, 6525 AJ, Nijmegen (The Netherlands)

† Shared first author.

* Corresponding authors: b.drobot@hzdr.de, lena.daumann@lmu.de

Abstract

Pyrroloquinoline quinone (PQQ) is a redox cofactor in calcium- and lanthanide-dependent alcohol dehydrogenases that has been known and studied for over 40 years. Despite its long history, many questions regarding its fluorescence properties, speciation in solution and in the active site of alcohol dehydrogenase remain open. Here we investigate the effects of pH and temperature on the distribution of different PQQ species (H_3PQQ to PQQ^{3-} as well as water adducts and in complex with lanthanides (Lns)) using NMR and UV-Vis spectroscopy as well as time-resolved laser-induced fluorescence spectroscopy (TRLFS). Using a europium derivative from a new, recently-discovered class of lanthanide-dependent methanol dehydrogenase (MDH) enzymes, we utilized two techniques to monitor Ln binding to the active sites of these enzymes. Using TRLFS, we were able to follow Eu(III) binding directly to the active site of MDH using its luminescence and could quantify three Eu states: Eu in the active site of MDH, but also in solution as PQQ-bound Eu and in the aquo-ion form. Additionally, we used the antenna effect to study PQQ and simultaneously Eu in the active site.

Introduction

During the past 20 years, the use of luminescent lanthanides (Lns) for biophysical studies of samples such as cells, proteins, DNA and biomarkers along with the use of luminescent lanthanide binding tags (LBT) for investigating protein interactions has increased dramatically.[1-6] The use of luminescent Lns such as Tb^{3+} and Eu^{3+} in proteins has so far been as substitutes for the native metal ions such as Ca^{2+}, Mg^{2+} or Co^{2+}.[7] However, with the advent of the new biological role of lanthanides for numerous bacteria (mostly methanotrophs and methylotrophs but other examples such as *P. putida*[8, 9] are known to encode Ln-dependent enzymes), it has now become possible to take advantage of the attractive photophysical properties of Ln in their natural biological environments.[10-14] The active sites of known lanthanide dependent enzymes (methanol dehydrogenases, MDH/XoxF, or ethanol dehydrogenase/ExaF, or alcohol dehydrogenase/PedH in *P. putida*) include the redox cofactor pyrroloquinoline quinone (PQQ) and an early Ln ion (La – Eu)[15] that is complexed by four amino acids bearing hard, negatively charged oxygen donors.[13, 16-18] For the MDH from *Methylacidiphilum fumariolicum* SolV (SolV) studied here, this corresponds to Glu172, Asn256, Asp299 and Asp301 (Figure 1).

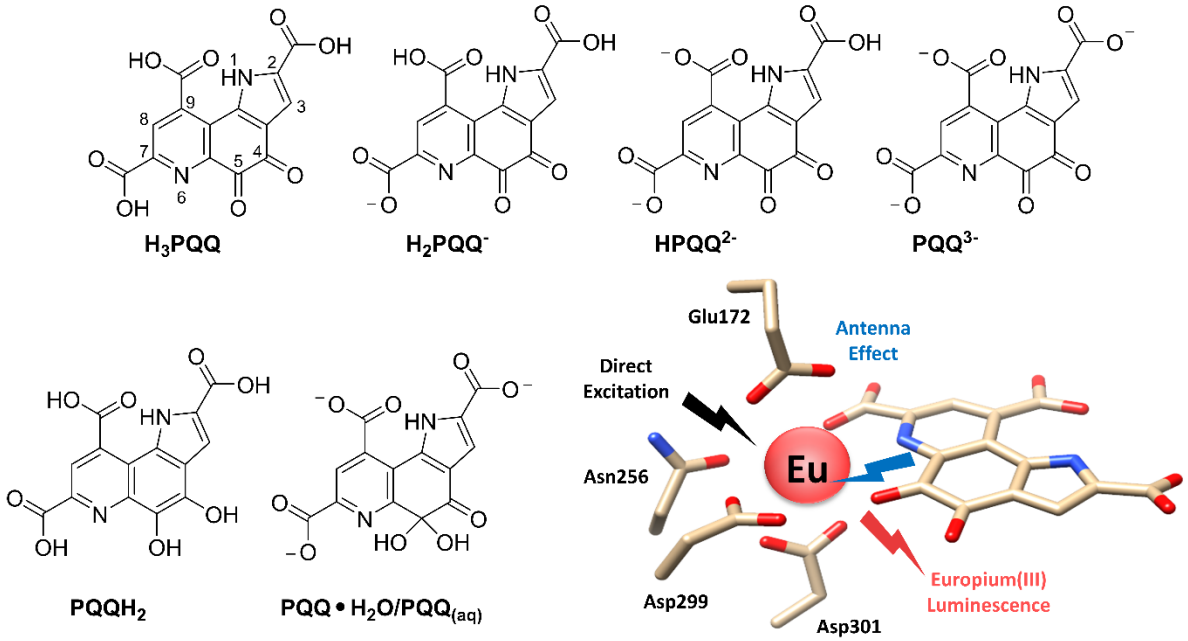

Figure 1 The protonation states of the different PQQ species discussed in this work are shown including the aromatic numbering scheme. The water adduct PQQ•H_2O, also referred to as $PQQ_{(aq)}$, forms readily in water with the various protonated states. The reduced diol form, $PQQH_2$, is the product after MeOH oxidation by MDH. When the protonation state: reduced, oxidized or semiquinone, is unknown, or the general form is of interest, we then refer to the cofactor as just "PQQ". Lower right. The Eu-MDH active site of *Methylacidiphilum fumariolicum* SolV is shown. The Eu-luminescence can be observed by either directly exciting Eu or using the antenna effect with PQQ.

The PQQ cofactor was first isolated and characterized by Anthony and Zatman in 1967.[19] Under aerobic conditions, free PQQ prevails in one of its oxidized ortho-quinone forms. Isolated PQQ readily adds nucleophiles at the C5 position, forming the water adduct PQQ•H_2O or a PQQ hemiketal species with alcohols (Figure 1).[20, 21] Formation of PQQ adducts with ammonia, cyanide and other components present in enzyme preparations have also been reported for PQQ within the MDH active site, each one of them with

a possibly different UV-Vis signature.[22-24] The exact position of the nucleophilic attack of water and methanol (MeOH) in free PQQ were studied by both experiment and theory.[25-27] Duine et al. reported a PQQ : PQQ•D_2O molar ratio of 2 : 1 in D_2O pD 6 solution.[25, 28] Unfortunately, the concentration, the temperature, or acquisition parameters for the NMR measurements were not included. A temperature-dependent equilibrium between PQQ and PQQ•H_2O, and its shift towards the latter at low temperatures was noticed by Dekker et al. when evaluating NMR, UV-Vis absorption and fluorescence spectra.[28] Although they determined the fractions of both components for at least two different temperatures, they did not compute biophysical parameters such as the equilibrium constant, reaction enthalpy or entropy. For Ca-MDH, Anthony described that a UV-Vis spectrum bearing an oxidized PQQ cofactor is inherently difficult to obtain and looks markedly different than the one with reduced cofactor $PQQH_2$.[29] Although the cofactor is non-covalently bound in the active site of the enzyme, it is difficult to reconstitute a PQQ-free active site of MDH. Multiple literature reports indicate that no 100% PQQ occupancy in the active site is observed. Moreover, the absence of this cofactor was seen in some of the crystal structures.[29-31] Here, the cofactor is usually refined in the structure using PQQ in the oxidized form.[30-33] However, it has been proposed that, in the case of Ca-MDH, the PQQ (directly after purification) is most likely in its semiquinone or reduced $PQQH_2$ state.[23, 29, 34] DFT-Calculations by Schelter and coworkers suggest that the semiquinone state is stable for Ce-MDH.[35] Taking all reports in the literature together, even after more than 50 years, the state of the cofactor in the active site of MDH remains, under certain conditions, undefined (H_3PQQ, H_2PQQ^-, $HPQQ^{2-}$, PQQ^{3-}, $PQQH_2$, semiquinone or any of the C5 adducts). Furthermore, most crystal structures, calculations and generic structure representations show PQQ with fully protonated carboxyl groups, corresponding to H_3PQQ, in the active site of MDH. However, the pK_a values suggest that, at physiological pH, at least the three carboxylic acids are deprotonated, thus PQQ^{3-}. Kano et al. determined PQQ's pK_a values in 0.5 M KCl solution by means of spectrophotometry as follows: 0.30 (N6), 1.60 (C7-COOH), 2.20 (C9-COOH), 3.30 (C2-COOH) and 10.30 (N1).[36] Considering the uncertainties regarding the protonation state, the form of the cofactor (oxidized, reduced, partially oxidized, adducts) and occupancy of PQQ in the active site, we set out to investigate these matters by exploiting not only the spectroscopic properties of PQQ but also those of europium(III), which is a direct binding partner in the active site. Analyzing PQQ fluorescence and Eu luminescence properties makes it possible to determine their photophysical properties within the active site of MDH and thereby distinguish the PQQ and Eu present at the MDH active site from the Eu aquo-ion and the Eu-PQQ bound species outside of the active site. Luminescence spectroscopy is a powerful tool to study the biochemistry of Eu(III) even at trace concentrations. From the emission spectra, we observe direct information about the changes in the local environment of Eu(III) and its interaction with PQQ. This was obtained via a parallel factor analysis (PARAFAC) of the time-resolved laser-induced luminescence spectroscopy (TRLFS) data as a tool for direct determination of the chemical species of Eu(III). Using the simultaneous analysis of multi-parameter data (pH dependency of the emission spectra and luminescence decay lifetime), we determined a unique model with three independent Eu(III) species. Furthermore, fluorescence spectroscopy was employed for a simultaneous lifetime characterization of the PQQ and the Eu in MDH active site.

Results and Discussion

PQQ Species in Solution

Acid Dissociation Constants of PQQ and PQQ•H_2O Species

PQQ (and its derivatives) exhibit a low solubility in water, especially in acidic media, with the solubility limit reported as 1.2×10^{-5} M for $H_3PQQ_{(aq)}$.[25, 27, 36] Thus, NMR spectroscopy of aqueous solutions is limited to ^{1}H nuclei. The ^{1}H NMR signal assignment to PQQ and PQQ•H_2O is explained in detail in the supporting information. Figure 2 shows the pH-titration spectra in the pH range 0.5 – 4 with increments of about 0.25 units, as well as the corresponding plot of the pH-dependent chemical shifts. For pK_a determination, sigmoidal (bi-)dose–response fits were applied to the data. As 3-H is closer to C2-COOH, the respective pK_a values (of ~ 3) were determined from corresponding data points in the pH range 1.25 – 4. The 8-H data sets reveal only one inflection for the pH range 0.5–2 25. Apparently, the pK_a values associated with the carboxyl groups bound to C7 and C9 are too close to be resolved, whereas the C2-COOH deprotonation is mirrored by 8-H. Accordingly, only two (*i.e.*, the lowest and highest) of the three carboxyl group associated pK_a values could be determined with sufficient certainty from the NMR titration. These values amount to 1.24 ± 0.04 and 3.02 ± 0.01 for PQQ, and 1.54 ± 0.04 and 3.10 ± 0.02 for PQQ•H_2O.

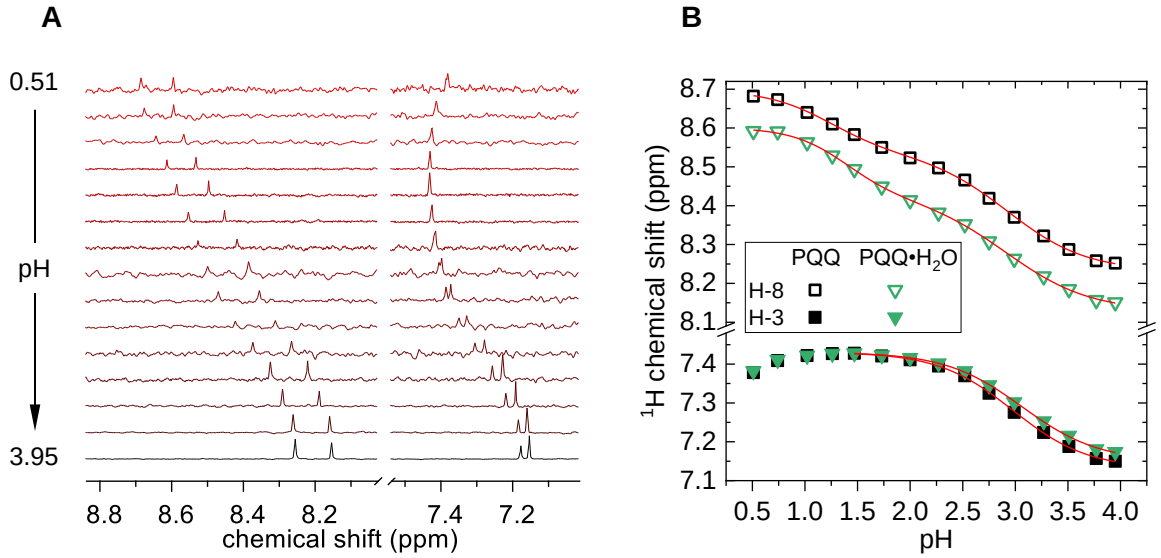

Figure 2 ^{1}H NMR pH-titration spectra (25 °C) of PQQ dissolved in 100 mM NaCl H_2O solution containing 10% D_2O (A), and the corresponding chemical shift vs. pH plot (B). The red lines correspond to sigmoidal (bi-)dose–response fits.

In addition to the NMR spectra, a UV-Vis series of 50 µM PQQ in 100 mM NaCl as a function of pH were recorded. The measured UV-Vis and deconvoluted single component spectra of the PQQ–water system are shown in Figure 3. We observe a strong shift of the UV absorption band from 363 to 333 nm in the acidic pH range. Furthermore, the absorption maximum at 248 nm shifts to 254 nm and the formation of shoulder at 275 nm becomes visible with increasing pH. Above pH 5, no further spectral changes are identifiable. Regarding the pH range and NMR results, PQQ can release three protons from the carboxylic groups at C2, C9 and C7. The calculated single component spectra of the four different aqueous species are shown

in Figure 3C. Based on the variation in the absorption spectra, by means of the program HypSpec[37, 38] the pK_a values were determined as pK_{a1} = 0.87 (C7-COOH), pK_{a2} = 1.67 (C9-COOH), and pK_{a3} = 3.17 (C2-COOH). The herein presented (lower) pK_a values obtained from 100 mM NaCl solutions are in fair agreement with those reported for 0.5 M KCl.[36] The differences are ascribed to different concentrations and the types of background electrolytes. The obtained data is fundamental for our subsequent pH-dependent metal-ion complexation investigations in aqueous solution. Protonation constants were also determined using the obtained fluorescence excitation–emission scans (Figure S1). Here, applying the PARAFAC analysis revealed the following pK_a values: pK_{a1} = 1.2 (C7-COOH), pK_{a2} = 1.35 (C9-COOH), and pK_{a3} = 3.4 (C2-COOH) that are in good agreement with the absorption data.

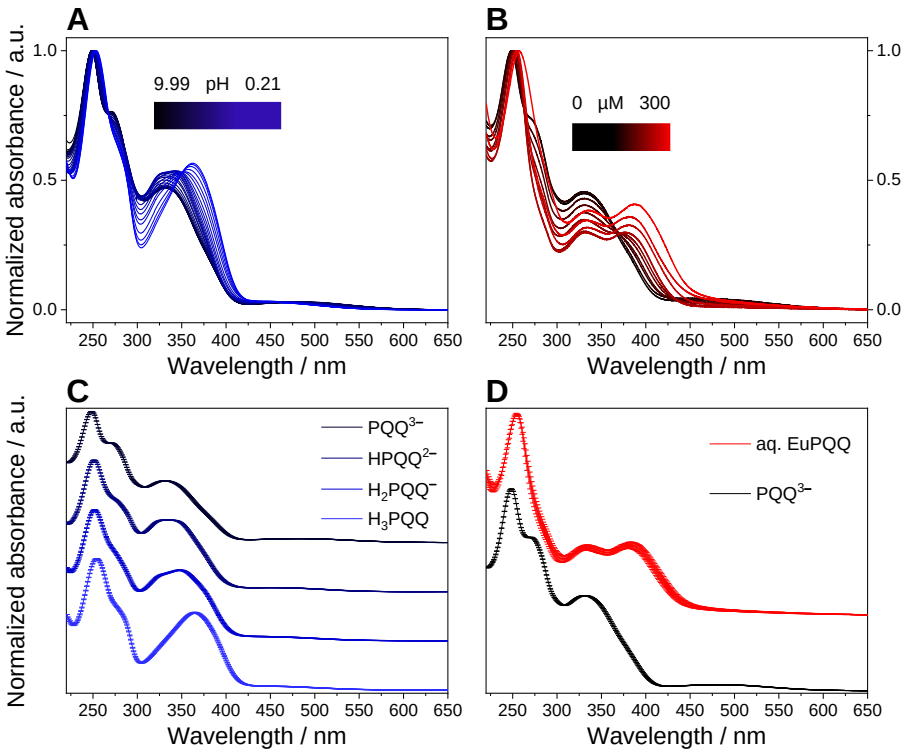

Figure 3 UV-Vis absorption spectra of the PQQ system: pH-titration series (A) and pH 6.5 Eu(III)-titration series (B) as well as corresponding single-component spectra obtained from spectral deconvolution for H_nPQQ^{n-3} protonation species (C) and free and Eu(III)-bound PQQ^{3-}, respectively. Concentration of total PQQ was 50 µM, that of Eu(III) was varied between 0 an 300 µM, respectively, in 100 mM NaCl aqueous solution.

Temperature- and pH-Dependence of the PQQ – PQQ•H_2O Equilibrium

The PARAFAC analysis was also used to follow the interconversion between PQQ^{3-} and its water adduct as a function of temperature. As previously reported, the fraction of PQQ increases with increasing temperature (Figure 4A-C).[28] At room temperature (and pH 6.5), both species occur roughly at a ratio of 1:1. The emission intensity of the PQQ^{3-} species is lower than that of the PQQ•H_2O^{3-} species (Figure 4E and F).

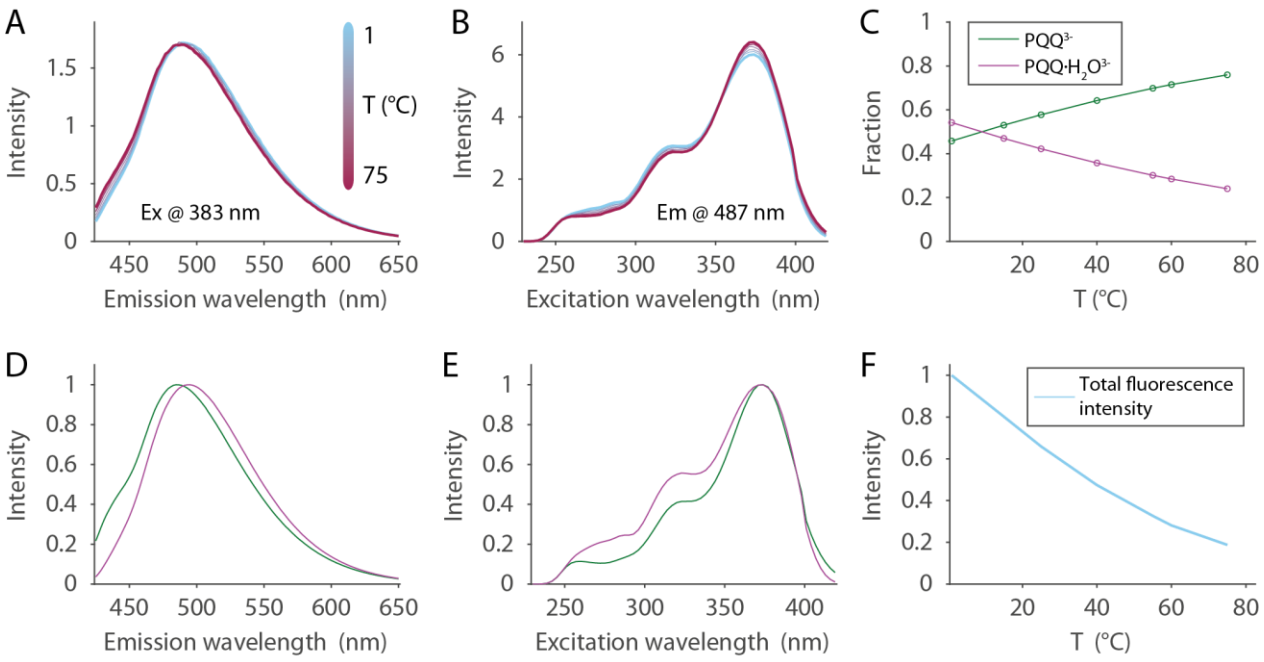

Figure 4 Fluorescence excitation–emission scans of a temperature series (1 to 75 °C) of 10 µM PQQ in aqueous 100 mM NaCl solution at pH 6.5. Minor changes in the normalized emission (A) and excitation (B) spectra at specific wavelengths are visible within the studied temperature range. The PARAFAC deconvolution provides two species. The distribution of PQQ^{3-} (green) and $PQQ{\bullet}H_2O^{3-}$ (magenta) is shown in (C), their individual emission spectra in (D) and excitation spectra in (E). The overall emission intensity decreases with temperature (F).

The temperature dependence of the chemical equilibrium between PQQ^{3-} and $PQQ{\bullet}H_2O^{3-}$ at pH 4.0 was investigated by variable temperature (VT-NMR) depicted in Figure S2A together with the corresponding van 't Hoff plot in Figure S2B. For the 1 mM pH 4.0 sample, the obtained enthalpy and entropy of hydration values are $\Delta_h H = (-13 \pm 1)$ kJ mol^{-1} and $\Delta_h S = (-47 \pm 2)$ J mol^{-1} K^{-1}, respectively. On the other hand, the obtained $\Delta_h H$ and $\Delta_h S$ values for the 0.5 mM pD 6.8 sample (VT-NMR spectra in Figure S2C) are −14 ± 1 kJ mol^{-1} and −51 ± 3 J mol^{-1} K^{-1}, respectively. Using the relative concentrations of both PQQ and $PQQ{\bullet}H_2O$ quoted by Dekker et al. determined for a pD 7 D_2O solution at 24 °C and 42 °C,[28] the respective values can be calculated as −15.2 kJ mol^{-1} and −55 J mol^{-1} K^{-1}, which fully agrees with our reported results. Since there were only these previous data for two different temperatures at one given pD, we have expanded our analysis allowing for a better data basis on the hydration reaction equilibrium. In addition, the obtained values are in line with literature thermodynamic parameters for the hydration reactions of other ketones.[39, 40] Consequently, the formation of $PQQ{\bullet}H_2O$ is mildly exothermic, favoring PQQ at elevated temperatures. In this regard, a decrease in the intensity of the NMR signals (3' and 8'), associated with a lower $PQQ{\bullet}H_2O$ concentration, was observed with increasing temperature. Likewise, an increase in the intensity of NMR signals (3 and 8) indicated an increase in the PQQ concentration. The quite negative entropy value is plausible as the number of free molecules reduces during the reaction. According to Buschmann et al.,[41] who studied hydration reactions of various aldehydes and ketones, the entropy contribution is about 25 J mol^{-1} K^{-1} per mole water involved in the reaction. It is thus concluded that, in addition to one water

molecule being the nucleophile that reacts with the carbonyl carbon, one more water molecule is required to stabilize the water adduct upon hydrogen bonding.

Investigations pertaining to the pH-dependence of the PQQ – PQQ•H_2O equilibrium allows for an advanced understanding of the principal reaction behavior of PQQ towards nucleophiles in general, and water in particular. At 25 °C, for pH < 2, PQQ•H_2O predominates, whereas for pH ≥ 2, PQQ predominates (Figure 5). Upon increasing pH, the PQQ•H_2O : PQQ ratio (equivalent to K_h) reveals a continuous decrease up to pH ~ 5, where the curve then flattens, approaching a K_h of about 0.55 in strongly alkaline medium. Although the hydration reaction (see statements for Water Adduct Equilibrium, SI) does not explicitly involve H^+, the pH apparently impacts the yield of the water adduct owing to the species-dependent electrophilicity of PQQ.

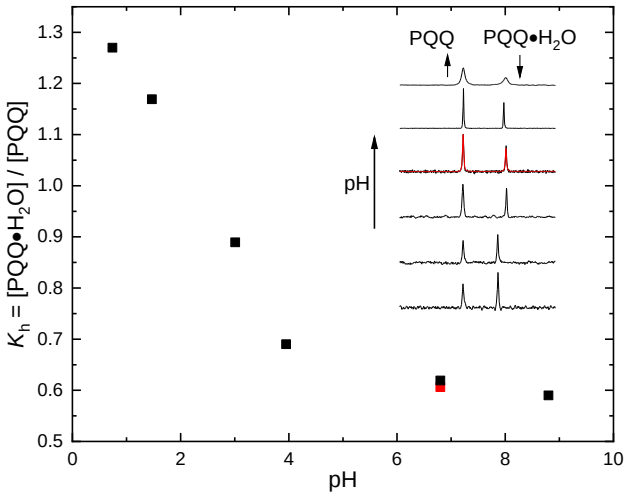

Figure 5. Plot showing the pH-dependence of the PQQ – PQQ•H_2O equilibrium at 25 °C as determined from pH-dependent ^{1}H NMR signal integrals of corresponding signals associated with 8-H (inset; arbitrary scaling). As the pH increases, the proportion of PQQ increases. Note the two data sets for pH 6.8: the total PQQ concentrations were 0.5 mM (black) and 5 mM (red) respectively.

Chemical Exchange Reaction Kinetics in the PQQ – PQQ•H_2O Equilibrium

NMR line shapes are sensitive to processes on the millisecond to microsecond time-scale, such as chemical exchange, since the inverse (in frequency units) covers the NMR spectral width. The observability of the very close signals 3 and 3' ($\Delta\nu$ = 15 Hz in acid solution, Figure S2A) is already a strong indication that the exchange is slow on the NMR time-scale, even at 60 °C. Thus, a first approximation for the exchange rate can be given as $k_{ex} \ll 15\ s^{-1}$. To qualitatively assess the dynamic equilibrium between PQQ and PQQ•H_2O in general, and to determine the exchange rate, 1D- and 2D-EXSY (exchange spectroscopy) spectra were acquired. The correlation signals caused by chemical exchange, unlike those due to the NOE (nuclear Overhauser effect), show the same phase (sign) as the diagonal signals. This can be seen at the dynamic equilibrium (pH 4.3 and 25 °C) in the 2D- and 1D-EXSY spectra (SI Figures S3 and S4, respectively), where the forward reaction yielding PQQ•H_2O proceeds with a rate of $0.9 \times 10^{-1}\ s^{-1}$ and the reverse reaction

yielding PQQ proceeds with a rate of 1.1×10^{-1} s^{-1}. Two further 2D-EXSY spectra with different mixing times were acquired at 60 °C. Assuming the exchange reaction will accelerate at 60 °C, mixing times of 125 and 400 ms were chosen for the experiments. From the 2D-EXSY, an exchange rate of k_{ex}(60 °C) = $(18.0 \pm 1.9) \times 10^{-1}$ s^{-1} was obtained indicating a 9-fold increase of the exchange rate for a temperature difference of 35 K.

Table 1 summarizes the complete set of temperature-dependent exchange rate constants $k_{ex}(T)$. Since both T_1 (see Table S1 and NMR Spectroscopy, SI) and k_{ex} notably increase upon increasing pH (see Table 1 and inset in Figure 6) where applicable, the exchange rate can be determined from the signals' line width, as applied to pD 6.8 spectra at different temperatures (Figure S2C and Table 1) as well as pH-dependent (25 °C) spectra (inset in Figure 6).

Table 1. Temperature-dependent exchange rate constants.

	$k_{ex}(T)$ / 10^{-1} s^{-1}	
T / °C	10 mM PQQ, pH 4.3	5 mM PQQ, pD 6.8
1		[c] 16 ± 2
15		[c] 19 ± 3
25	[a] 2.0 ± 0.1	[c] 21 ± 4
		[b] 22 ± 1
35	[b] 2.7 ± 0.1	[c] 63 ± 9
		[b] 70 ± 5
45	[b] 5.6 ± 0.1	[c] 135 ± 24
		[b] 127 ± 7
55		[c] 273 ± 33
60	[a] 18.0 ± 1.9	
	[b] 18.0 ± 0.4	

[a] 2D-^{1}H,^{1}H-EXSY; [b] selective excitation 1D-EXSY; [c] Line width analyses

Plotting ln($k_{ex}(T)/T$) vs. $1/T$ results in the graph shown in Figure S5, from which the following values were calculated using Eqn S5: $\Delta H^{\ddagger} = (50 \pm 6)$ kJ mol^{-1} and $\Delta S^{\ddagger} = (-91 \pm 18)$ J mol^{-1} K^{-1} for 10 mM pH 4.3 solution, and $\Delta H^{\ddagger} = (66 \pm 4)$ kJ mol^{-1} and $\Delta S^{\ddagger} = (-17 \pm 13)$ J mol^{-1} K^{-1} for 5 mM pD 6.8 solution, respectively corresponding to $\Delta G^{\ddagger}$ (25 °C) values of 78 and 71 kJ mol^{-1}. The significantly lower $\Delta S^{\ddagger}$ determined for the pH 4.3 solution indicates a higher requirement for water solvation in the transition state than in the diol. The absolute value itself corresponds to four water molecules involved for pH 4.3 while for pD 6.8 only one water molecule is critical (according to 25 J mol^{-1} K^{-1} per mole water[41]). This can be

interpreted as a highly ordered cyclic hydrogen-bonded transition state at pH 4.3, involving three water molecules, one of which is the nucleophile (Figure S6A) plus one additional water for solvation. In contrast, at pD 6.8, the hydroxide ion, being the better nucleophile, can directly attack the C5 carbonyl carbon even when only present in small concentrations.

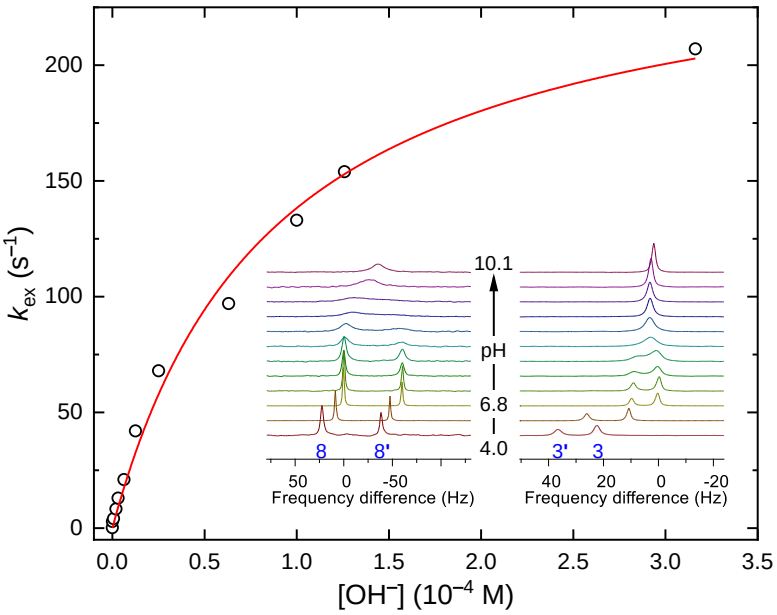

Figure 6. Plot showing the pH-dependent rate of PQQ – PQQ•H_2O interconversion as determined from line shape analyses at 25 °C. The pH 6.8 spectrum serves as reference since both forms occur exclusively in their tri-anionic species, so no additional protonation–deprotonation dynamics have to be considered. Note the larger frequency difference between signals 8 and 8' compared to 3 and 3' at low pH (i.e., for slow exchange) causes the latter signal pair to coalesce (merge) earlier for a given pH-dependent rate.

To sum up, PQQ undergoes hydration *via* two different, pH-dependent mechanisms. From a thermodynamic point of view, the increased enthalpy of activation (corresponding to the activation energy, E_a, in collision theory) impedes PQQ•H_2O formation, mirroring the shift of the equilibrium towards PQQ upon increasing pH. From a kinetic point of view, however, the cyclic transition state requires all involved molecules to rearrange with high demands on the geometry, slowing down the reaction rates for both hydration and dehydration. With increasing pH, *i.e.* increasing the concentration of OH^-, the nucleophile can directly attack the carbonyl group *via* formation of a tetrahedral transition state (Figure S6B) with much less geometric demands (much less negative $\Delta S^{\ddagger}$). Apparently, the reaction rates accelerate notably (Figure 6). However, not only for the forward reaction yielding PQQ•H_2O, but also for the reverse reaction, *i.e*. dehydration, yielding PQQ. Comparing pH 4.3 and pD 10.1, the interconversion rates increases by three orders of magnitude, but their ratio r_{hyd}/r_{deh} corresponding to the PQQ•H_2O : PQQ ratio = K_h (see Eqns. S4 and S8 in the SI), changes only from ~ 0.7 to ~ 0.55 (asymptotic approach).

PQQ and Europium in Methanol Dehydrogenase

After gathering a thorough understanding of PQQ, its protonation states, and its equilibrium with the corresponding C5 water adduct PQQ•H_2O, we analyzed the properties and behavior of PQQ and Eu(III) within Eu-MDH. We have observed that the Eu-MDH enzyme readily loses PQQ during storage and washing procedures and that the Eu(III) occupancy in the MDH sample is around 70% as shown per ICP-OES.[31, 42] Other groups have also reported complete loss of PQQ (or metal ion) in Ln-MDH crystal structures.[30] To gain further insight into the possible PQQ species and their interconversion in the active site of MDH, the impact of temperature (5 °C to 50 °C) and the presence of the substrate MeOH on the absorption spectra of Eu-MDH (Figure 7) was studied. Note, the ratio of 'free' PQQ in solution to PQQ•H_2O is 1:1 at 5 °C and shifts to 3:1 at 55 °C. The typical PQQ fingerprint was observed in all collected spectra of MDH isolated from the methanotrophic bacterium SolV (Figure 7). As previously described for Eu-MDH isolated from SolV, this species displays an absorption maximum at 355 nm and a shoulder at 400 nm.[31] Interestingly, depending on the presence or absence of MeOH, we see two opposite trends of the PQQ fingerprint absorbance values at 355 nm and 400 nm upon heating. In the absence of MeOH, a small increase of the signal at 355 nm is first observed followed by the reduction of the signal with increasing temperature. The shoulder at 400 nm increases slowly at first but, when 40 °C is reached, this band intensifies (Figure 7A). For Eu-MDH supplemented with MeOH, the spectra show a small increase in the peak at 355 nm while the absorbance at 400 nm remains unchanged (Figure 7B). For both Eu-MDH samples, the described changes in spectra appear starting around 35 °C to 40 °C and intensify with elevating temperature.

The two observed peaks at 355 nm and 400 nm indicate different states of the prosthetic group. In the beginning of the experiment, the main PQQ species might be the semiquinone or the quinol form, independent of MeOH addition, since an absorbance at 355 nm is clearly visible. As described by Goodwin and Anthony, spectra of MDH with and without Ca^{2+} differ, however both spectra reveal the concurrent presence of different states of PQQ indicated by varying intensity of the peaks at 345 and 400 nm.[43, 44] In the inactive apo form (without Ca^{2+}), it was suggested that PQQ is mainly present in its oxidized form since strong absorbance at 400 nm is detected. [43, 45] Subsequent metal addition reveals an increased reduced state of PQQ, which is observed by an increase of the absorbance at 345 nm.[43, 45] The shoulder observed at 400 nm in our data suggests that some PQQ is present in the oxidized form. At temperatures above 35 °C in the presence of the substrate MeOH, the amount of reduced $PQQH_2$ or half reduced PQQH• radical species might increase. This is supported by the fact that these changes start to occur around 35 °C, which is the minimum temperature for substrate conversion. At temperatures below 35 °C, no or little enzymatic activity is observed for Eu-MDH. Above 40 °C, the signal at 355 nm decreases while the signal at 400 nm increases. Compared to literature, this points to a decrease of the $PQQH_2$ or PQQH• state whereas, at the same time, more oxidized PQQ is present. Since the experiments were conducted under an ambient atmosphere, O_2 might serve as a terminal oxidant at elevated temperatures. To sum up, although a clear identification of the state of the redox cofactor is not possible, and as the MDH likely contains a mixture of PQQ species, the results indicate that both temperature and MeOH have a significant influence on the state of PQQ within MDH.

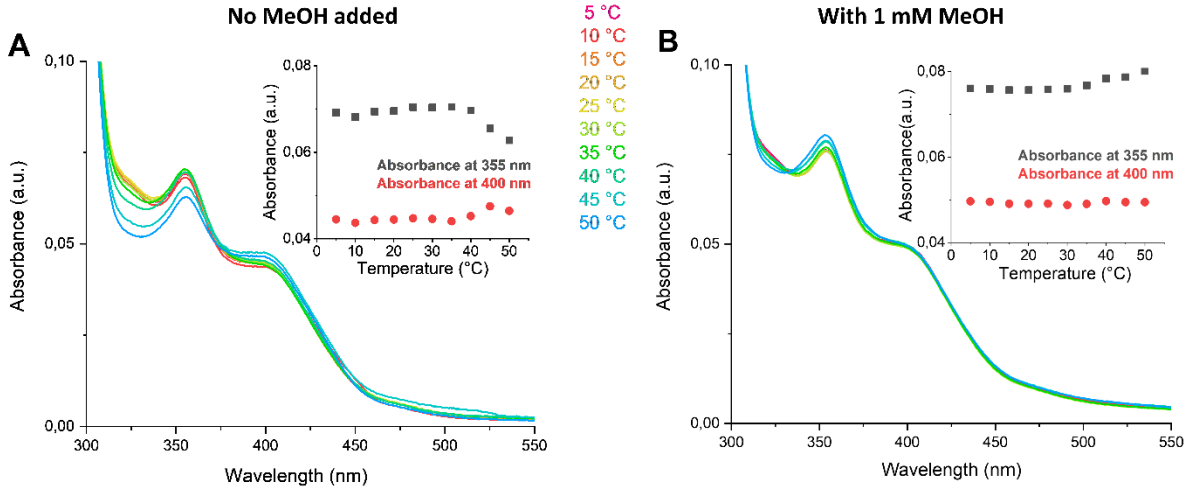

Figure 7. Normalized temperature-dependent UV-Vis spectra of Eu-MDH in 100 mM NaCl, pH 6.5 solution recorded in the absence **A** and in the presence **B** of 1 mM MeOH. The corresponding absorbance values at 355 nm and 400 nm are highlighted in the insets.

Determination of the different Eu(III) species by TRLFS

The titration of Eu(III) to a partial Ln-apo MDH purified from SolV (where 70% europium content was determined by ICP-OES) can restore complete enzymatic activity.[31, 46] Addition of Lns results in a gradual increase in enzymatic activity and, upon 100% occupation of the active site, a saturation behavior can be observed.[46] Titrations of Eu(III) to Eu-MDH (with only partially occupied Eu-sites) using TRLFS with a direct excitation of Eu(III) at 394 nm were thus used to directly probe the different Eu(III) species. Prior to the TRLFS experiments, we checked the effect of the laser irradiation on the Eu-MDH to choose the desired laser power that does not destroy the probed sample (Figure S7). To avoid additional Eu-buffer complex species, this experiment was carried out in non-buffered NaCl solution. For the titration experiments, two solutions were prepared: 10 µM Eu-MDH (with only partially occupied Eu-sites) and 3 mM $EuCl_3$ both in 100 mM NaCl at pH 6.5. In one titration, 1 mM MeOH was added (see Experimental section in the Supporting Information for details). During the titration, both the symmetry-forbidden F_0 transition peak and the F_2 transition decreased. This is already an indication that the Eu(III) aquo ion concentration is increasing during the titration (Figure 8A). PARAFAC explains 98.3 % of the variance in the spectrum using a three species model, as shown for the emission spectrum of 40 µM $EuCl_3$ (Figure S8). The extracted spectra for the three Eu(III) species is shown in Figure 8: the Eu(III) aquo ion is shown in green, the active site-bound Eu(III) in magenta and a third Eu(III) species in yellow, which could not be assigned to a specific binding site at the enzyme. The assignment of the Eu(III) aquo ion is straightforward. The green emission spectrum provides the typical F_1/F_2 ratio, the lifetime is 111 µs and its concentration increases with higher Eu(III) concentration. The assignment of the active site-bound Eu(III) spectra (magenta) is supported by ICP-OES measurements, which reveal a fraction of approximately 70% MDH being occupied by Eu(III). This is in good agreement with the population of the magenta species present at the beginning of the titration, before

Eu(III) was added. The maximal increase of about 25% in the magenta distribution indicates a similar initial occupation as determined previously by ICP-OES.[31] The prolonged luminescence decay time of 290 µs for this species indicates a highly coordinated environment. By means of the Horrocks equation,[47-50] the remaining number of coordination water molecules is determined to be 3. The pronounced F_0 transition (increased emission at ~ 580 nm) results from an asymmetric Eu(III) coordination environment, which further supports the assignment of the magenta species to the Eu-MDH complex. To identify the third, yellow species, we decided to compare it with Eu(III) complexed to PQQ. Both emission spectra have a similar shape (Figure S9) and show unusually short lifetimes (75 µs for the third species (yellow), 88 µs for the Eu-PQQ complex), which have to be caused by quenchers other than water. The third species (yellow) was therefore assigned to Eu(III) bound to PQQ, which we found to readily dissociate from the active site of MDH upon washing and explains the decreasing specific activities during sample handling and storage on ice over a day (or even during crystallization). From the titration graph, a dissociation constant of 3.2×10^{-6} for the active site-bound Eu (magenta) was calculated (Figure 8C). This is in good agreement with Eu(III) interactions with other proteins, e.g. calmodulin ($4 \times 10^{-8} – 4 \times 10^{-5}$).[51]

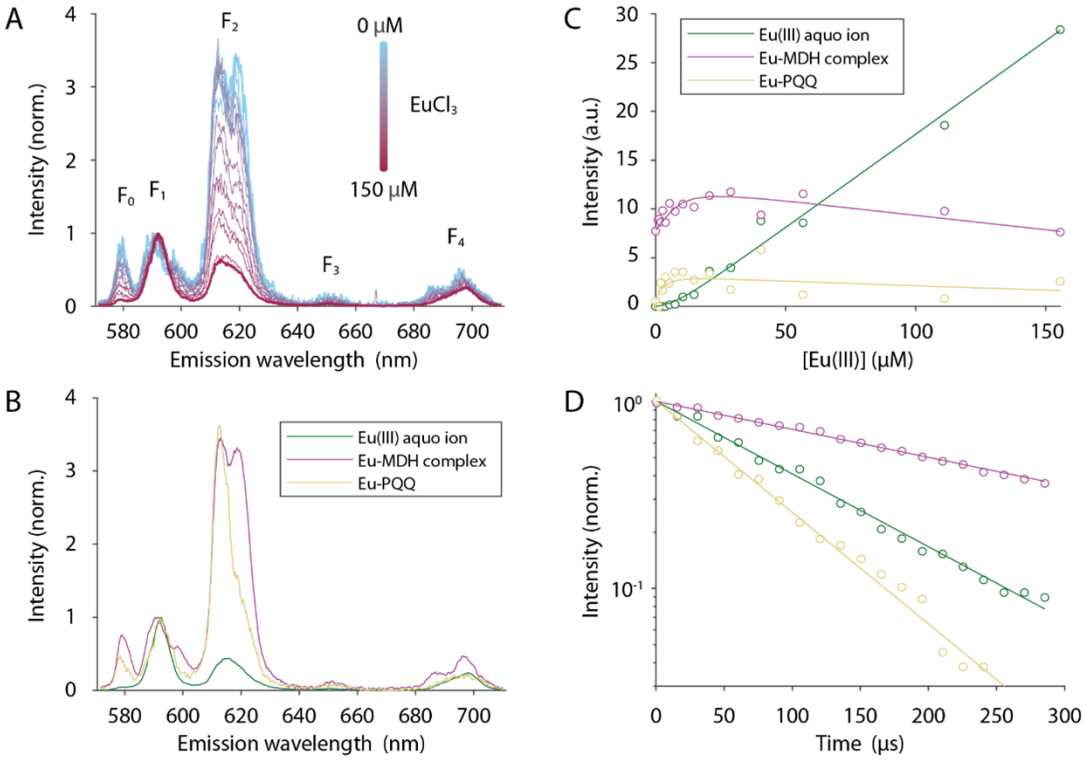

Figure 8. TRLFS of an Eu(III) titration to the MDH. **A** The emission spectra of the Eu(III) titration series for t = 0 µs normalized to the emission of F_1. **B - D** Results from the PARAFAC analysis. **B** Emission spectra of the three chemical species that are formed during the Eu(III) titration (normalized to the emission of F_1). The spectra were assigned to the Eu(III) aquo ion (green), Eu(III) in the active site of MDH (magenta) and a Eu-PQQ complex (yellow) formed in buffer from dissociated PQQ. **C** The corresponding distribution of the three different Eu(III) species and **D** their luminescence decays. The decrease in intensity of the magenta and yellow species is caused by sample dilution during the Eu(III) titration.

PQQ proximity to Eu in the Eu-MDH active site

After thoroughly investigating the photophysical properties of both PQQ and Eu(III), we sought to utilize the antenna effect by directly exciting PQQ and measuring the luminescence emission and lifetimes from both the PQQ and the Eu(III) bound in the active site (Figure 9A). Before measuring in the protein, we first characterized the PQQ and Eu interactions in buffer. We directly excited PQQ at 375 nm and measured the emission signal and lifetime properties of both the PQQ and the Eu (Figure 9B-D). The energy transfer from PQQ (excited state) to the Eu in its proximity is demonstrated by both the steady state luminescence emission spectrum and the lifetime measurements. A decrease in the fluorescence emission of PQQ in the presence of 1 mM Eu is observed along with a concomitant increase in the induced electric dipole transition $^5D_0 \rightarrow {}^7F_2$ of Eu (Figure S10). We also observed a decrease of the fluorescence lifetime of the PQQ•H_2O : PQQ species in the presence of 1 mM Eu due to energy transfer from PQQ to Eu (Figure S10D). Interestingly, under the conducted experimental conditions (20 mM PIPES pH 7.2 at 22 °C), the PQQ measurement in buffer, which is a mixture of PQQ•H_2O : PQQ (ratio ~ 0.6 as shown in Figure 5), shows a mono-exponential lifetime of ~ 1.3 ns, which suggests that both PQQ species have similar fluorescence lifetimes.

For measurements with MHD, not only the presence of metal in the MDH active site influences the emission and fluorescence lifetime properties of the PQQ but also the properties of the Ln ion present. Hence, we measured the luminescence emission spectra and lifetimes of PQQ and Eu for both Eu-MDH and La-MDH. A characterization of PQQ–La interactions in buffer is summarized in Figure S11. The luminescence emission spectrum for Eu-MDH shows the induced electric dipole transition $^5D_0 \rightarrow {}^7F_2$ peak in Eu-MDH, as expected, which is absent in the case of La-MDH (Figure 9B).

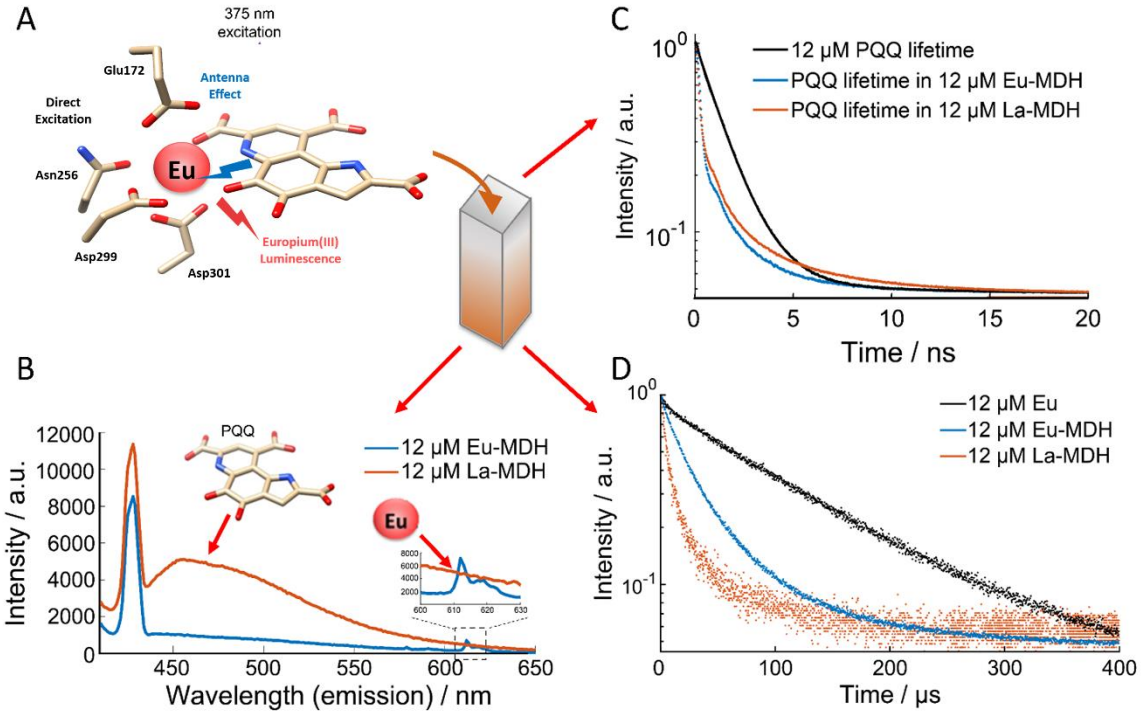

Figure 9 Spectroscopic investigations of PQQ and Eu in the MDH active site. A) The antenna effect between PQQ and Eu in the active site of MDH is investigated by exciting the PQQ directly with 375 nm light. B) The steady-state luminescence emission spectra from 375 nm excitation of PQQ in the presence of 12 µM Eu-MDH and 12 µM La-MDH. The $^5D_0 \rightarrow {}^7F_2$ transition of Eu is clearly visible around 615 nm in the presence of Eu-MDH. C) The fluorescence lifetime of PQQ monitored at 495 nm alone in solution and in the presence of 12 µM Eu-MDH and 12 µM La-MDH. D) The lanthanide luminesce lifetime monitored at 620 nm for 12 µM Eu in solution as well as for 12 µM Eu-MDH and 12 µM La-MDH.

We also observed quenching in the PQQ fluorescence lifetime distribution for both Eu-MDH and La-MDH (Figure 9C), which is a further indication of the PQQ proximity to the lanthanide atom present in the active site of the protein. The quenching effect of Eu on PQQ in the active site is stronger than for La-MDH suggesting a better energy transfer from the PQQ excited state to Eu (Figures S9A and S10A). This is consistent to what was observed for Eu-PQQ and La-PQQ interactions in buffer. The fluorescence intensity of PQQ at 495 nm as a function of PQQ concentration is $(1.50 \pm 0.19) \times 10^4\ \mu M^{-1}$ in the presence of 1 mM La versus $(1.41 \pm 0.18) \times 10^3\ \mu M^{-1}$ in the presence of 1 mM Eu (Figures S9C and S10C). The higher transfer efficiency between PQQ and Eu is the main reason why the PQQ fluorescence is less prominent in Eu-MDH compared to La-MDH (Figure 9B). Another factor influencing the PQQ fluorescence in the MDH is the occupancy of the metal ion in the MDH active site, which is around 70% for the Ln-MDH samples but was observed to vary among the several sample preparations (Figure S12). To verify that the effect we are observing is specific to MDH, we monitored the spectral and lifetime changes of both the PQQ fluorescence and the Ln luminescence in Eu-MDH and La-MDH before and after its denaturation with Hellmanex III (Figure S13A). First, we verified that 2% Hellmanex III had no effect on the spectral and lifetime behavior of PQQ in the absence of Eu-MDH (Figure S14). Denaturation of Eu-MDH showed that the PQQ fluorescence emission spectrum is recovered due to the absence of Eu in its proximity after denaturation. Similarly, the lifetime of PQQ returns to 1.3 ns upon denaturation (Figure S13B). Hence, there is a clear energy transfer between PQQ and the Ln metal ion, which are in close proximity in the active site of the MDH.

Conclusion

The thorough characterization of PQQ and the effect of pH and temperature on the different PQQ species that are formed confirms the importance of a detailed PQQ understanding prior to investigating its presence in methanol dehydrogenase enzymes. We studied the different PQQ species in solution by using NMR and UV-Vis spectroscopy and proceeded by investigating PQQ in the Eu-MDH active site by combining fluorescence spectroscopy techniques; TRLFS, and luminescence emission and lifetime measurements. In solution, we showed that PQQ and its species, H_3PQQ to PQQ^{3-}, complex with Lns and form water adducts as well. Using TRLFS, excitation of the Eu(III) at 395 nm was possible, which enabled a direct investigation of the Eu species present in purified MDH. Through this approach, we determined that three different Eu(III) species exist in a Eu-MDH environment. Next to the aquo-Eu present in solution, we determined the amount of Eu(III) bound to PQQ and the Eu(III) present in the MDH active site. The latter is essential for understanding the photophysical properties of the Eu-MDH and we could also show that MDH can loose

PQQ from the active site, a phenomenon also observed by other researchers working with MDH. In addition, we utilized the fluorescence of PQQ and the luminescence of Eu(III) as a tool to simultaneously monitor the photophysical features of the Eu-MDH. The proximity of the PQQ to the Eu(III) in the active site leads to energy transfer and its effect on the Eu luminescent properties can be investigated using the antenna effect by the direct excitation of PQQ using a 375 nm laser. The luminescence spectra and quenching can be useful tools for investigating metal-cofactor interactions within biomolecules in general and Ln-PQQ interactions in Ln-containing proteins in particular.

Conflicts of interest

There are no conflicts to declare.

Acknowledgements

We thank Heidrun Neubert and Dominik Goldbach (HZDR) for their support in the lab. LJD would like to acknowledge a grant from the Deutsche Forschungsgemeinschaft (DFG, German Research Foundation)-392552271. DCL gratefully acknowledges the financial support of the Deutsche Forschungsgemeinschaft (DFG, German Research Foundation) – Project-ID 201269156 – SFB 1032 Project B03 as well as the Ludwig-Maximilian University, Munich via the Center for NanoScience (CeNS) and the LMUinnovativ initiative BioImaging Network (BIN).

References FIXME

1. E. G. Moore, A. P. S. Samuel and K. N. Raymond, *Accounts of Chemical Research*, 2009, **42**, 542-552.
2. K. N. Allen and B. Imperiali, *Current Opinion in Chemical Biology*, 2010, **14**, 247-254.
3. J. W. Walton, A. Bourdolle, S. J. Butler, M. Soulie, M. Delbianco, B. K. McMahon, R. Pal, H. Puschmann, J. M. Zwier, L. Lamarque, O. Maury, C. Andraud and D. Parker, *Chemical Communications*, 2013, **49**, 1600-1602.
4. S. J. Butler, L. Lamarque, R. Pal and D. Parker, *Chemical Science*, 2014, **5**, 1750-1756.
5. K. Binnemans, *Coordination Chemistry Reviews*, 2015, **295**, 1-45.
6. T. J. Sorensen, A. M. Kenwright and S. Faulkner, *Chemical Science*, 2015, **6**, 2054-2059.
7. C. H. Evans, *Biochemistry of the Lanthanides*, Springer Science & Business Media, New York, 1990.
8. M. Wehrmann, C. Berthelot, P. Billard and J. Klebensberger, *mSphere*, 2018, **3**, e00376-00318.
9. M. Wehrmann, P. Billard, A. Martin-Meriadec, A. Zegeye and J. Klebensberger, *mBio*, 2017, **8**, e00570-00517.
10. E. Skovran and N. C. Martinez-Gomez, *Science*, 2015, **348**, 862-863.
11. L. Chistoserdova, *World Journal of Microbiology & Biotechnology*, 2016, **32**, 138-+.
12. J. A. Cotruvo, *Acs Central Science*, 2019, **5**, 1496-1506.
13. L. J. Daumann, *Angewandte Chemie-International Edition*, 2019, **58**, 12795-12802.
14. N. Picone and H. J. M. Op den Camp, *Current Opinion in Chemical Biology*, 2019, **49**, 39-44.
15. H. Lumpe, A. Pol, H. J. M. Op den Camp and L. J. Daumann, *Dalton Trans.*, 2018, **47**, 10463-10472.
16. N. M. Good, H. N. Vu, C. J. Suriano, G. A. Subuyuj, E. Skovran and N. C. Martinez-Gomez, *Journal of Bacteriology*, 2016, **198**, 3109-3118.

17. M. Wehrmann, P. Billard, A. Martin-Meriadec, A. Zegeye and J. Klebensberger, *Mbio*, 2017, **8**.
18. R. A. Schmitz, N. Picone, H. Singer, A. Dietl, K.-A. Seifert, A. Pol, M. S. M. Jetten, T. R. M. Barends, L. J. Daumann and H. J. M. Op den Camp, *mBio*, 2021, **12**, e0170821-e0170821.
19. C. Z. L. J. Anthony, *Biochem. J*, 1967, **104**, 953-959.
20. H. Lumpe and L. J. Daumann, *Inorg. Chem.*, 2019, **58**, 8432-8441.
21. S. Itoh, M. Ogino, Y. Fukui, H. Murao, M. Komatsu, Y. Ohshiro, T. Inoue, Y. Kai and N. Kasai, *Journal of the American Chemical Society*, 1993, **115**, 9960-9967.
22. J. A. Duine and J. Frank, Jr, *Biochemical Journal*, 1980, **187**, 213-219.
23. J. Frank, M. Dijkstra, J. A. Duine and C. Balny, *European Journal of Biochemistry*, 1988, **174**, 331-338.
24. T. K. Harris and V. L. Davidson, *Biochemistry*, 1993, **32**, 4362-4368.
25. J. A. Duine, J. Frank and P. E. J. Verwiel, *Eur. J. Biochem.*, 1981, **118**, 395-399.
26. Y.-J. Zheng and T. C. Bruice, *Proc. Natl. Acad. Sci.*, 1997, **94**, 11881.
27. H. Lumpe and L. J. Daumann, *Inorg. Chem.*, 2019, **58**, 8432-8441.
28. R. H. Dekker, J. A. Duine, J. Frank, J. P. E. J. Verwiel and J. Westerling, *Eur. J. Biochem.*, 1982, **125**, 69-73.
29. C. Anthony, *Subcellular Biochemistry*, 2000, **35**, 73-117.
30. N. M. Good, M. Fellner, K. Demirer, J. Hu, R. P. Hausinger and N. C. Martinez-Gomez, *Journal of Biological Chemistry*, 2020, **295**, 8272-8284.
31. B. Jahn, A. Pol, H. Lumpe, T. R. M. Barends, A. Dietl, C. Hogendoorn, H. J. M. Op den Camp and L. J. Daumann, *Chembiochem*, 2018, **19**, 1147-1153.
32. Y. W. Deng, S. Y. Ro and A. C. Rosenzweig, *J. Biol. Inorg. Chem.*, 2018, **23**, 1037-1047.
33. A. Pol, T. R. M. Barends, A. Dietl, A. F. Khadem, J. Eygensteyn, M. S. M. Jetten and H. J. M. O. d. Camp, *Environ. Microbiol.*, 2014, **16**, 255-264.
34. M. Dijkstra, J. Frank, Jr and J. A. Duine, *Biochemical Journal*, 1989, **257**, 87-94.
35. J. A. Bogart, A. J. Lewis and E. J. Schelter, *Chem. – Eur. J.*, 2014, **21**, 1743–1748.
36. K. Kano, K. Mori, B. Uno, T. Kubota, T. Ikeda and M. Senda, *Bioelectrochem. Bioenerg.*, 1990, **24**, 193-201.
37. P. Gans, A. Sabatini and A. Vacca, *Annali Di Chimica*, 1999, **89**, 45-49.
38. P. Gans, A. Sabatini and A. Vacca, *Talanta*, 1996, **43**, 1739-1753.
39. H.-J. Buschmann, H.-H. Füldner and W. Knoche, *Ber. Bunsenges. Phys. Chem.*, 1980, **84**, 41-44.
40. P. Greenzaid, Z. Rappoport and D. Samuel, *Trans. Faraday Soc.*, 1967, **63**, 2131-2139.
41. H.-J. Buschmann, E. Dutkiewicz and W. Knoche, *Ber. Bunsenges. Phys. Chem.*, 1982, **86**, 129-134.
42. B. Jahn, N. S. W. Jonasson, H. Hu, H. Singer, A. Pol, N. M. Good, H. J. M. O. den Camp, N. C. Martinez-Gomez and L. J. Daumann, *JBIC Journal of Biological Inorganic Chemistry*, 2020.
43. C. Anthony, in *Enzyme-Catalyzed Electron and Radical Transfer: Subcellular Biochemistry*, eds. A. Holzenburg and N. S. Scrutton, Springer US, Boston, MA2000, pp. 73-117.
44. M. G. Goodwin and C. Anthony, *Biochemical Journal*, 1996, **318**, 673-679.
45. M. G. Goodwin, A. Avezoux, S. L. Dales and C. Anthony, *Biochemical Journal*, 1996, **319**, 839-842.
46. H. Lumpe, A. Pol, H. J. M. Op den Camp and L. J. Daumann, *Dalton Trans.*, 2018, **47**, 10463-10472.
47. W. D. Horrocks and D. R. Sudnick, *Journal of the American Chemical Society*, 1979, **101**, 334-340.
48. T. Kimura and Y. Kato, *J. Alloys Compd.*, 1998, **275–277**, 806-810.
49. P. P. Barthelemy and G. R. Choppin, *Inorg. Chem.*, 1989, **28**, 3354-3357.
50. T. Kimura and G. R. Choppin, *J. Alloys Compd.*, 1994, **213-214**, 313-317.
51. B. Drobot, M. Schmidt, Y. Mochizuki, T. Abe, K. Okuwaki, F. Brulfert, S. Falke, S. A. Samsonov, Y. Komeiji, C. Betzel, T. Stumpf, J. Raff and S. Tsushima, *Physical Chemistry Chemical Physics*, 2019.